A., & Ishii, H., Eds.) pp 87-90, Elsevier, Amsterdam.
Jeffery, J., Cederlund, E., & Jörnvall, H. (1984) *Eur. J. Biochem. 140*, 7-16.
Jones, T. A. (1985) *Methods Enzymol. 115*, 157-171.
Jones, T. A., & Thirup, S. (1986) *EMBO J. 5*, 819-822.
Juliâ, P., Parês, X., & Jörnvall, H. (1988) *Eur. J. Biochem. 172*, 73-83.
Jörnvall, H. (1985) *Alcohol 2*, 61-66.
Jörnvall, H., Eklund, H., & Brändén, C.-I. (1978) *J. Biol. Chem. 253*, 8414-8419.
Jörnvall, H., Hempel, J., Vallee, B. L., Bosron, W. F., & Li, T.-K. (1984) *Proc. Natl. Acad. Sci. U.S.A. 81*, 3024-3028.
Jörnvall, H., Persson, B., & Jeffery, J. (1987) *Eur. J. Biochem. 167*, 295-201.
Jörnvall, H., Persson, B., Krook, M., & Hempel, J. (1991) in *The Molecular Pathology of Alcoholism* (Palmer, N., Ed.) pp 130-156, Oxford University Press, Oxford, England.
Kaiser, R., Holmquist, B., Hempel, J., Vallee, B. L., & Jörnvall, H. (1988) *Biochemistry 27*, 1132-1140.
Kaiser, R., Holmquist, B., Vallee, B. L., & Jörnvall, H. (1989) *Biochemistry 28*, 8432-8438.
Kaiser, R., Nussrallah, B. A., Dam, R., Wagner, F. W., & Jörnvall, H. (1990) *Biochemistry 29*, 8365-8371.
Koivusalo, M., Baumann, M., & Uotila, L. (1989) *FEBS Lett. 257*, 105-109.
Laemmli, U. K. (1970) *Nature 227*, 680-685.
Lange, L. G., & Vallee, B. L. (1976) *Biochemistry 15*, 4681-4686.
Lange, L. G., Sytkowski, A. J., & Vallee, B. L. (1976) *Biochemistry 15*, 4687-4693.
Moreno, A., & Parês, X. (1991) *J. Biol. Chem. 266*, 1128-1133.
Parês, X., Moreno, A., Cederlund, E., Höög, J.-O., & Jörnvall, H. (1990) *FEBS Lett. 277*, 115-118.
Pryor, A., & Huppatz, J. L. (1982) *Biochem. Int. 4*, 431-438.
Tapia, O., Brändén, C.-I., & Armbruster, A.-M. (1982) in *Quantum Theory of Chemical Reactions*, Vol. 3, pp 97-123, Reidel, Dordrecht, The Netherlands.
Theorell, H. (1970) in *Pyridine Nucleotide-Dependent Dehydrogenases* (Sund, H., Ed.), pp 121-128, Springer-Verlag, Berlin and New York.
Vallee, B. L., & Bazzone, T. J. (1983) *Isozymes: Curr. Top. Biol. Med. Res. 8*, 219-244.
Wagner, F. W., Burger, A. R., & Vallee, B. L. (1983) *Biochemistry 22*, 1857-1863.
Yasunami, M., Chen, C.-S., & Yoshida, A. (1991) *Proc. Natl. Acad. Sci. U.S.A. 88*, 7610-7614.
Yin, S.-J., Vagelopoulos, N., Wang, S.-L., & Jörnvall, H. (1991) *FEBS Lett., 283*, 85-88.
Yoshida, A., Hsu, L., & Yasunami, M. (1991) in *Alcoholism. A Molecular Perspective* (Palmer, T. N., Ed.) pp 95-99, Plenum Press, New York.

Quantitation of Lateral Stress in Lipid Layer Containing Nonbilayer Phase Preferring Lipids by Frequency-Domain Fluorescence Spectroscopy†

Sun-Yung Chen,‡ Kwan Hon Cheng,*,‡ and B. Wieb Van Der Meer§
Department of Physics, Texas Tech University, Lubbock, Texas 79409, and Department of Physics and Astronomy, Western Kentucky University, Bowling Green, Kentucky 42101

Received August 20, 1991; Revised Manuscript Received January 24, 1992

ABSTRACT: Frequency-resolved fluorescence measurements have been performed to quantitate the lateral stress of the lipid layer containing nonbilayer phase preferring dioleoylphosphatidylethanolamine (DOPE). On the basis of a new rotational diffusion model, the wobbling diffusion constant (D_w), the curvature-related hopping diffusion constant (D_H), and the two local orientational order parameters ($\langle P_2 \rangle$ and $\langle P_4 \rangle$) of 1-palmitoyl-2-[[2-[4-(6-phenyl-*trans*-1,3,5-hexatrienyl)phenyl]ethyl]carbonyl]-3-*sn*-phosphatidylcholine (DPH-PC) in fully hydrated DOPE and DOPE/dioleoylphosphatidylcholine (DOPC) mixtures were calculated from the frequency-domain anisotropy data. The values of $\langle P_2 \rangle$, $\langle P_4 \rangle$, and D_H for DOPE were found to increase significantly at ~12 °C, the known lamellar liquid crystalline (L_α) to inverted hexagonal (H_{II}) phase transition temperature of DOPE. Similar features as well as a decline of D_w were detected in the DOPE/DOPC mixtures as the DOPE content was increased from 85% to 90% at 23 °C, corresponding to the known lyotropic phase transition of the DOPE/DOPC. In contrast, for DOPC (0-40 °C) and DOPE/DOPC (0-100% DOPE at 3 °C), which remained in the L_α phase, ese changes were not detected. The most probable local orientation of DPH-PC in the DOPE/DOPC mixtures shifted progressively toward the normal of the lipid/water interface as the content of DOPE increased. We concluded that the curvature-related lateral stress in the lipid layer increases with the content of the nonbilayer phase preferring lipids.

The structural morphologies of the lipids in the lamellar liquid crystalline (L_α) and inverted hexagonal (H_{II}) phases have been recognized and established (Luzzati & Husson, 1962; Cheng & Hui, 1986; Tate & Gruner, 1989; Rand et al., 1990). In the L_α phase, the molecules are arranged in stacked lipid bilayers with sheets of water between the polar surfaces of the lipids. However, in the H_{II} phase, the molecules rearrange themselves to form long water-cored cylindrical tubes in which the lipid polar head groups are facing the long symmetric axes of the cylinders. The L_α to H_{II} phase transition involves a change in the lipid/water surface curvature and a

† This work was supported by grants from the National Institutes of Health (CA 47610) and the Robert A. Welch Research Foundation (D-1158) to K.H.C.
* Address correspondence to this author at Biophysics Laboratory, Department of Physics, Texas Tech University, Lubbock, TX 79409.
‡ Texas Tech University.
§ Western Kentucky University.

0006-2960/92/0431-3759$03.00/0

topologically discontinuous rearrangement of the lipids.

The role of nonbilayer phase preferring lipids in the function of biological membranes has been a subject of interest for many years (Cheng & Hui, 1986; Cheng, 1989a; Gruner, 1989). Recently, a *stress* model has been proposed (Gruner, 1989). Within the context of this model, the curvature-related lateral stress is a major physiochemical factor which dictates the bilayer to nonbilayer phase transition of the lipids. It is further argued that the stress is also present and already developed within the bilayer of cell membranes, which contain the nonbilayer phase preferring lipids, irrespective of whether the nonbilayer structures actually exist or not. This hypothesized building up of lateral stress in the lipid layer has not been tested experimentally by fluorescence spectroscopy. This study aimed at quantitating the lateral stress in the lipid layer containing nonbilayer phase preferring lipids by frequency-domain spectroscopic technique (Cheng, 1989a–c; Gratton et al., 1984).

Two simple lipid systems were employed in this study. They are the pure lipid suspensions of either dioleoylphosphatidylethanolamine (DOPE) or dioleoylphosphatidylcholine (DOPC), as a function of temperature, and the binary mixtures of DOPE/DOPC as a function of DOPE content at 3 and 23 °C. These lipid systems have been investigated extensively by the X-ray diffraction technique (Gruner, 1989; Rand et al., 1990). DOPE has the L_α–H_{II} phase transition temperature at 8–12 °C. DOPC does not have the L_α–H_{II} transition, but it has the same fatty acyl chain composition as does DOPE. For DOPE/DOPC at 23 °C, a lyotropic (composition dependent) L_α–H_{II} phase transition occurs at 85–90% PE. However, no phase transition is found at 3 °C.

Recently, a new rotational diffusion model (Van Der Meer et al., 1990) was developed to investigate the orientational dynamics of the lipids in the curved H_{II} phase. The application of this model in studying lipids with well-defined L_α and H_{II} phases has recently been initiated (Van Der Meer et al., 1990; Chen et al., 1990a). On the basis of this new rotational diffusion model (Van Der Meer et al., 1990), we planned to investigate both the local orientational order and rotational dynamics of the above lipid systems by measuring the frequency-domain fluorescence anisotropy of 1-palmitoyl-2-[[2-[4-(6-phenyl-*trans*-1,3,5-hexatrienyl)phenyl]ethyl]-carbonyl]-3-*sn*-phosphatidylcholine (DPH-PC) in the above lipid systems. DPH-PC is structurally similar to a phosphatidylcholine lipid except that one of its hydrocarbon chains consists of a 1,6-diphenyl-1,3,5-hexatriene (DPH) fluorophore connected to the *sn*-2 position of the glycerol backbone via a short propanoyl chain. The photophysical properties of this DPH-PC are almost identical to that of DPH (Parente & Lentz, 1985; Cheng, 1989a).

The validity of our rotational model was also tested by comparing our fluorescence results with the known structural parameters of the lipids. A hopping diffusion coefficient (D_H) which describes the rotational diffusion of the fluorophore over a curved surface is introduced in the model. This parameter is related with the translational diffusion coefficient (D_L) of the probe and the radius of curvature of the surface (Van Der Meer et al., 1990). The values of D_L have also been measured separately by the pyrene excimer formation technique (Chong & Thompson, 1985; Chen et al., 1990b). A pyrene-labeled lipid was used for this lateral diffusion measurement. From the values of D_H and D_L, the radii of curvature of the lipids in the known H_{II} phase were estimated and compared with the same parameters obtained from the X-ray diffraction measurements (Rand et al., 1990).

Finally, from the reconstructed orientational distribution function of DPH-PC, we attempted to establish the existence of the curvature-related lateral stress in the lipid layer containing nonbilayer phase preferring lipids.

Materials and Methods

Sample Preparation

1,2-Dioleoylphosphatidylcholine (DOPC) and 1,2-dioleoylphosphatidylethanolamine (DOPE) were obtained from Avanti Polar Lipids (Birmingham, AL). Fluorescent lipids, DPH-PC and 1-palmitoyl-2-[10-(1-pyrenyl)decanoyl]-PC (PyPC), were obtained from Molecular Probes, Inc. (Eugene, OR). All lipids were dissolved in chloroform and stored at −80 °C prior to use.

For the frequency-domain fluorescence lifetime and anisotropy measurements, the molar ratio of DPH-PC to lipid was 1:1000. For the lateral diffusion measurements, two different molar ratios of PyPC to lipid were used, 5:10000 for the intrinsic pyrene monomer fluorescence lifetime measurement and 2:100 for the pyrene excimer formation rate constant measurement. Each lipid mixture was dried under a gentle nitrogen stream in a clean pyrex tube and further kept in vacuum for at least 4 h to ensure complete removal of chloroform. The thin film formed on the tube was then hydrated with an aqueous buffer (100 mM NaCl, 10 mM TES, and 2 mM EDTA, pH 7.4) at 4 °C. The suspension thus formed was vortexed rigorously and placed under mild sonication in a bath sonicator for a few seconds. The resulting suspension was then incubated overnight at 4 °C in the dark to ensure proper hydration. Upon further dilution to ≈0.1 mg/mL, the sample was then placed in a 10-mm UV quartz cuvette for subsequent fluorescence measurements. To eliminate oxygen quenching in pyrene excimer formation measurements, the buffer was purged with dry nitrogen gas before use. Also the sample chamber of the fluorometer was purged continuously with dry nitrogen during the fluorescence measurements to avoid water condensation at low temperatures.

Frequency-Domain Fluorescence Intensity and Anisotropy Measurements

All frequency-domain fluorescence measurements were performed on a frequency-domain cross-correlation fluorometer (ISS Inc., Champaign, IL) using a Liconix 4240NB cw He–Cd laser (Santa Clara, CA) with an output of 17 mW at 325 nm as the excitation source. The operational principle of this fluorometer has been described in detail elsewhere (Lakowicz, 1983; Gratton et al., 1984).

The fluorescence lifetime of DPH-PC was measured by using a nonfluorescent glycogen solution as a reference sample. Since the light exiting from the pockels cell (electro-optical device) is vertically polarized, a polarizer with its polarization axis set at 35° with respect to the vertical was placed in the excitation beam in order to eliminate the contribution of the rotational diffusion effect of the sample to the measurements (Spencer & Weber, 1970). A low wavelength cut-off filter (model 3-72, Corning Glass Works, Corning, NY) was used to remove the excitation light from the fluorescent signal. Both the phase delay ($\delta_F - \delta_S$) and modulation ratio (M_F/M_S) were measured at different modulation frequencies ranging from 1 to 300 MHz. Here δ_F and δ_S represent the phase delay of the signal from the fluorescent sample and that from the reference sample, respectively, and M_F and M_S represent the intensity modulation values of the fluorescent sample and that of the reference, respectively.

The fluorescence lifetime of PyPC monomer was measured at 380 nm through a monochromator (slit width = 2.0 nm).

Both the phase delay and the modulation ratio of the PyPC fluorescence signal were compared with that of a standard solution [1,4-bis[2-(5-phenyloxazolyl)]benzene (POPOP) in ethanol, lifetime = 1.34 ns] and measured at different modulation frequencies ranging from 100 kHz to 10 MHz.

For the fluorescence anisotropy measurements of DPH-PC, both excitation and emission polarizers were used (same emission filter as described above). The differential polarized phase angle ($\delta_\perp - \delta_\parallel$) and ratio of polarized modulation amplitudes ($M_\parallel/M_\perp$) were measured at different modulation frequencies (1–300 MHz). The subscripts $\parallel$ and $\perp$ refer to the directions of the polarization axis of the emission polarizer that are parallel and perpendicular to the vertical axis, respectively.

Data Analysis

(*a*) *Frequency-Domain Data Analysis.* In general, the time-resolved fluorescence intensity decay [$I(t)$] of a fluorescent sample can be expressed by a sum of exponential decays, i.e.,

$$I(t) = \sum_i^n \alpha_i e^{-t/\tau_i} \quad (1)$$

In the above expression τ_i and α_i are the fluorescence lifetime and the preexponential factor of the ith component, and n is the total number of components. In the frequency-domain measurements, τ_i and α_i can be calculated from the values of ($\delta_F - \delta_S$) and (M_F/M_S) (Weber, 1977).

The time-resolved fluorescence emission anisotropy decay $r(t)$ of a fluorescence sample can also be determined from the frequency-domain method. From the definition of $r(t)$, the decays of the parallel ($I_\parallel$) and perpendicular ($I_\perp$) components of the fluorescence emission can be represented as

$$I_\parallel(t) = \frac{1}{3}I(t)[1 + 2r(t)] \quad (2)$$

$$I_\perp(t) = \frac{1}{3}I(t)[1 - r(t)] \quad (3)$$

In the frequency-domain method, the differential polarized phase angle ($\delta_\perp - \delta_\parallel$) and the ratio of polarized modulation amplitudes ($M_\parallel/M_\perp$) are related to the above polarization decays.

(*b*) *Fluorescence Anisotropy Decay Models.* Using an interpolation theory (Van Der Meer et al., 1984; Szabo, 1984), the $r(t)$ of a cylindrical fluorophore in the L_α phase has been derived. In the case where the fluorophore satisfies (a) the absorption and/or emission dipole are close to the molecular long axis (Zannoni et al., 1983) or (b) the axial rotation along the long symmetry axis is much faster than the wobbling motion perpendicular to the long symmetry axis (Cheng, 1989a), one has $r(t) = r_0 Q_W$, with

$$Q_W = r_0[\langle P_2\rangle^2 + (1 - \langle P_2\rangle^2)\exp[-6D_W t/(1 - \langle P_2\rangle^2)]] \quad (4)$$

where r_0 is the initial anisotropy, Q_W is defined as the depolarization factor due to wobbling, $\langle P_2\rangle$ is the second rank order parameter, and D_W is the wobbling diffusion constant with respect to an axis which is perpendicular to the long axis of the probe. As seen in eq 4, $r(t)$ has the form of a constant plus an exponential. Equation 4 is denoted as the P2 model.

A higher order approximation of $r(t)$ has also been derived (Van Der Meer et al., 1984), where

$$r(t) = r_0 Q_W = r_0[\langle P_2\rangle^2 + \beta_{00}\exp(-\alpha_{00}t) + 2\sum_{m=1}^{2}\beta_{m0}\exp(-\alpha_{m0}t)] \quad (5)$$

The exponents (α_{m0}) and preexponentials (β_{m0}) are functions of $\langle P_2\rangle$, $\langle P_4\rangle$, and D_W, and are shown below.

m	β_{m0}
0	$1/5 + 2\langle P_2\rangle/7 + 18\langle P_4\rangle/35 - \langle P_2\rangle^2$
1	$1/5 + \langle P_2\rangle/7 - 12\langle P_4\rangle/35$
2	$1/5 - 2\langle P_2\rangle/7 + 3\langle P_4\rangle/35$
m	α_{m0}
0	$6D_W(1/5 + \langle P_2\rangle/7 - 12\langle P_4\rangle/35)/\beta_{00}$
1	$6D_W(1/5 + \langle P_2\rangle/14 + 8\langle P_4\rangle/35)/\beta_{10}$
2	$6D_W(1/5 - \langle P_2\rangle/7 - 2\langle P_4\rangle/35)/\beta_{20}$

Here $\langle P_4\rangle$ is the fourth rank order parameter. Equation 5 is denoted as the P2P4 model.

In the case of the H_{II} phase, a model for $r(t)$ that includes the combined effect of the lateral diffusion over a cylindrical surface (hopping) and of the wobbling diffusion has recently been derived (Van Der Meer et al., 1990). This model requires the assumption that the fluorescence depolarization due to hopping and that due to wobbling of the fluorophore are independent. This is equivalent to saying that the combined depolarization effects of the hopping and wobbling motions of the fluorophore in a curved surface result in a product of Q_W and Q_H in the expression for $r(t)$. The factor Q_H has been derived as

$$Q_H = \frac{1}{4} + \frac{3}{4}\exp(-4D_L t/R^2) = \frac{1}{4} + \frac{3}{4}\exp(-4D_H t) \quad (6)$$

where D_L is the lateral diffusion constant, R is the radius of curvature of the lipid layer, and D_H ($= D_L/R^2$) is defined as the curvature-related hopping diffusion constant. In the case of the lipids in the H_{II} phase, this R is measured from the center of the water cylinder to the emission dipole of the fluorophore inside the hydrocarbon region of the lipid layer. Using the expression of Q_W as given by eq 4, $r(t)$ can be expressed as

$$r(t) = r_0 Q_W Q_H = \frac{r_0}{4}[\langle P_2\rangle^2 + 3\langle P_2\rangle^2\exp(-t/\tau_H) + (1 - \langle P_2\rangle^2)\exp(-t/\tau_W) + 3(1 - \langle P_2\rangle^2)\exp[-(\tau_W + \tau_H)t/\tau_W\tau_H]] \quad (7)$$

where τ_H and τ_W are defined as $R^2/4D_L$ and $(1 - \langle P_2\rangle^2)/(6D_W)$, accordingly. Equation 7 is called the P2HOP model. It contains three molecular parameters, i.e., D_W, $\langle P_2\rangle$, and D_H.

If the second approximation of Q_W, i.e., eq 5, is used, a new expression for $r(t)$ which contains one more order parameter ($\langle P_4\rangle$) can be obtained. Now $r(t)$ takes the form of

$$r(t) = (r_o/4)[\langle P_2\rangle^2 + B_o\exp(-C_o t)][1 + 3\exp(-t/\tau_H)] + B_1\exp(-C_1 t)[\exp(-t/4\tau_H) + \exp(-t/\tau_H)] + (B_2/4)\exp(-C_2 t)[3 + 4\exp(-t/4\tau_H) + \exp(-t/\tau_H)] \quad (8)$$

The factors B_i and C_i ($i = 0, 1, 2$) are functions of $\langle P_2\rangle$, $\langle P_4\rangle$, and τ_W and are shown below.

i	B_i
0	$1/5 + 2\langle P_2\rangle/7 + 18\langle P_4\rangle/35 - \langle P_2\rangle^2$
1	$1/5 + \langle P_2\rangle/7 - 12\langle P_4\rangle/35$
2	$1/5 - 2\langle P_2\rangle/7 + 3\langle P_4\rangle/35$
i	C_i
0	$(1 - \langle P_2\rangle^2)(1/5 + \langle P_2\rangle/7 - 12\langle P_4\rangle/35)/B_0\tau_W$
1	$(1 - \langle P_2\rangle^2)(1/5 + \langle P_2\rangle/14 + 8\langle P_4\rangle/35)/B_1\tau_W$
2	$(1 - \langle P_2\rangle^2)(1/5 - \langle P_2\rangle/7 - 2\langle P_4\rangle/35)/B_2\tau_W$

Equation 8 is called the P2P4HOP model. Note that the P2P4HOP is a general model for both the L_α and H_{II} phases. The P2P4 model for the L_α phase (eq 5) can be considered as the limiting case of the P2P4HOP model when D_H approaches to zero. This occurs as R approaches infinity, i.e., the cylindrical surface degenerates into a planar surface.

(*c*) *Data Minimization.* A nonlinear least-squares fit procedure utilizing the Marquardt algorithm for minimizing the value of χ^2 was employed to determine the values of r_0, $\langle P_2 \rangle$, $\langle P_4 \rangle$, D_W, and D_H from the frequency-domain anisotropy data. For the frequency-domain data analysis, χ^2 is defined as the sum of the square of deviations between the observed and expected phase and modulation values of the fluorescence measurements over all the modulation frequencies. Usually this χ^2 is further divided by the total degrees of freedom of the fitting, i.e., the number of experimental data minus the number of fitting parameters, in order to obtain the reduced chi-square, χ_R^2. A detailed description of the frequency-domain fitting procedure and the estimation of the fitting errors has been described elsewhere (Gratton et al., 1984; Cheng, 1989a).

(*d*) *Orientation Distribution Function Determination.* The orientation of a cylindrical fluorophore in a lipid matrix is described by an orientational distribution function $f(\theta)$, where θ is defined as the polar angle between the long molecular symmetry axis of the fluorophore and the normal of the lipid/water interface. The distribution function $f(\theta)$ can be expressed as a series expansion of Legendre polynomials $[P_L(\cos\theta)]$ (van Langen et al., 1989).

$$f(\theta) = \frac{1}{2}\sum_{L=0}^{\infty}(2L+1)\langle P_L\rangle P_L(\cos\theta) \tag{9}$$

In the expansion, each polynomial is weighted by an order parameter $\langle P_L \rangle$ of order L. The function $f(\theta)$ obeys the normalization condition, i.e.,

$$\int_0^{\pi} f(\theta)\sin\theta\, d\theta = 1 \tag{10}$$

On the basis of the orthogonal property of Legendre polynomials, $\langle P_L \rangle$ can be expressed as

$$\langle P_L\rangle = \int_0^{\pi} f(\theta)P_L(\cos\theta)\sin\theta\, d\theta \tag{11}$$

Due to the symmetric nature of the distribution function, only the even Legendre polynomials contribute to the summation in eq 9. In practice, only one or two order parameters can be resolved experimentally on a macroscopically nonoriented crystals and in oriented crystals (Szabo, 1984; Cheng, 1989a). Nevertheless, the form of the $f(\theta)$ can be estimated on the basis of the values of the recovered order parameters $\langle P_2 \rangle$ and $\langle P_4 \rangle$ by using information theory (Jaynes, 1983; Berne et al., 1968; Ameloot et al., 1984; Deinum et al., 1988) and has the form of

$$f(\theta) = N^{-1}\exp[\lambda_2 P_2(\cos\theta) + \lambda_4 P_4(\cos\theta)] \tag{12}$$

where N is a normalization constant and λ_2 and λ_4 are the corresponding coefficients for the Legendre polynomial P_2 and P_4. The values of λ_2, λ_4, and N can be obtained from the known values of $\langle P_2 \rangle$ and $\langle P_4 \rangle$ according to eq 11 and the normalization condition of $f(\theta)$ as given by eq 10, i.e.,

$$\langle P_2\rangle = \int_0^{\pi} N^{-1}\exp[\lambda_2 P_2(\cos\theta) + \lambda_4 P_4(\cos\theta)]P_2(\cos\theta)\sin\theta\, d\theta \tag{13}$$

$$\langle P_4\rangle = \int_0^{\pi} N^{-1}\exp[\lambda_2 P_2(\cos\theta) + \lambda_4 P_4(\cos\theta)]P_4(\cos\theta)\sin\theta\, d\theta \tag{14}$$

$$N = \int_0^{\pi}[\lambda_2 P_2(\cos\theta) + \lambda_4 P_4(\cos\theta)]\sin\theta\, d\theta \tag{15}$$

From the values of λ_2, λ_4, and N, the orientational distribution function $f(\theta)$ can therefore be reconstructed from eq 12.

(*e*) *Lipid Lateral Diffusion Constant Measurement.* The lateral diffusion constant (D_L) of the lipids can be estimated by measuring the monomer fluorescence lifetimes of PyPC at two different concentrations, 0.05 and 2% (PyPC/lipid molar ratio).

Using a classical random walk model (Galla et al., 1979) and assuming that the excimer dissociation rate is much slower than the excimer association rate of the fluorophore, D_L has the form of

$$\langle n_s\rangle = \frac{2}{\pi X_{py}}\ln\left(\frac{2}{X_{py}}\right)\frac{L^2}{4}(\tau^{-1} - \tau_0^{-1}) \tag{16}$$

Here τ and τ_0 are the fluorescence lifetimes of pyrene monomer in the presence and absence of excimer formation, respectively. These lifetimes were determined from the samples containing 2 and 0.05% PyPC, accordingly. Also X_{py} is the pyrene/lipid molar ratio and is equal to 0.02 in our case.

Results

Frequency-Domain Fluorescence Anisotropy Measurements of DPH-PC in Pure DOPE and DOPC Suspensions. Frequency-domain fluorescence anisotropy measurements of DPH-PC in both DOPC and DOPE suspensions were performed by the use of multifrequency cross-correlation phase-modulation technique from 0 to 40 °C. Fluorescence lifetimes of DPH-PC are required for calculating the moleculr dynamics parameters from the frequency-domain data (Lakowicz, 1983). These lifetimes were also measured by the use of phase-modulation technique. Using a single-exponential fit, the fluorescence lifetimes of DPH-PC were found to be around 6 ns in both DOPC and DOPE suspensions and independent of temperature (0–40 °C). A better fit was obtained by using a double-exponential decay function as judged by the observation that the reduced χ^2 value of the double-exponential fit was smaller than that of the single-exponential fit. In this case, a major long lifetime component at ~6.2 ns and a shorter lifetime component (1–2 ns) with an intensity fraction less than 0.04 were found for both lipid suspensions. The extra short lifetime has been attributed to the minor but unavoidable degraded product of the fluorescent probe as described in detail elsewhere (Parente & Lentz, 1985; Cheng, 1989a–c). There are no detectable differences in the calculated rotational and orientational parameters obtained by using either the single- or double-exponential decay function of DPH-PC in the analysis of the frequency-domain fluorescence anisotropy data (Cheng, 1989a–c).

Figure 1A shows the typical frequency-domain anisotropy data of DPH-PC and DOPE at 30 °C. Both P2HOP and P2 models were employed to fit the data. In general we observed that the values of χ_R^2 from the P2HOP fit were quite similar to those from the P2 fit for DOPC at all temperatures (0–40 °C) and DOPE at low temperatures (<20 °C). However, for DOPE at high temperatures (>20 °C), an almost 2-fold decrease in the values of χ_R^2 from the P2HOP fit than those from the P2 fit was found. Using the higher order approximation models, the values of χ_R^2 from the P2P4HOP fit were also smaller than those from the P2P4 fit for DOPE at high temperatures. Again, no improvements in the values of χ_R^2 were observed for DOPC at all temperatures and for DOPE at low temperatures. The P2HOP (or P2P4HOP) therefore represents a better model than the P2 (or P2P4) in describing the fluorescence anisotropy decay behavior of DPH-PC in DOPE at high temperatures. Table I shows the typical values of the fitted parameters and their corresponding reduced chi-squares (χ_R^2) from the P2, P2HOP, P2P4, and P2P4HOP models for

Table I: Comparison of the Results from the P2, P2HOP, P2P4, and P2P4HOP Fits for DPH-PC in DOPE and DOPC at 30 °C[a]

	r_0	$\langle P_2 \rangle$	$\langle P_4 \rangle$	D_w (10^7 s^{-1})	D_H (10^7 s^{-1})	χ_R^2
DOPE	0.24 ± 0.01	0.62 ± 0.01		2.65 ± 0.03	N/A	2.94[b]
	0.24 ± 0.02	0.85 ± 0.02		2.40 ± 0.20	1.90 ± 0.13	1.34[c]
	0.24 ± 0.01	0.59 ± 0.03	−0.07 ± 0.04	4.00 ± 0.15	N/A	1.71[d]
	0.24 ± 0.02	0.82 ± 0.03	0.52 ± 0.10	4.70 ± 1.80	1.80 ± 0.18	1.12[e]
DOPC	0.28 ± 0.02	0.54 ± 0.02		3.12 ± 0.06	N/A	2.21[b]
	0.27 ± 0.03	0.62 ● 0.04		3.63 ± 0.56	0.16 ± 0.09	2.06[c]
	0.27 ± 0.01	0.50 ± 0.04	−0.25 ± 0.03	4.52 ± 0.26	N/A	2.22[d]
	0.27 ± 0.01	0.51 ± 0.04	−0.24 ± 0.08	4.87 ± 0.12	0.07 ± 0.41	2.90[e]

[a] The fitting errors are also shown. [b] Fitting obtained from the P2 model. [c] Fitting obtained from the P2HOP model. [d] Fitting obtained from the P2P4 model. [e] Fitting obtained from the P2P4HOP model.

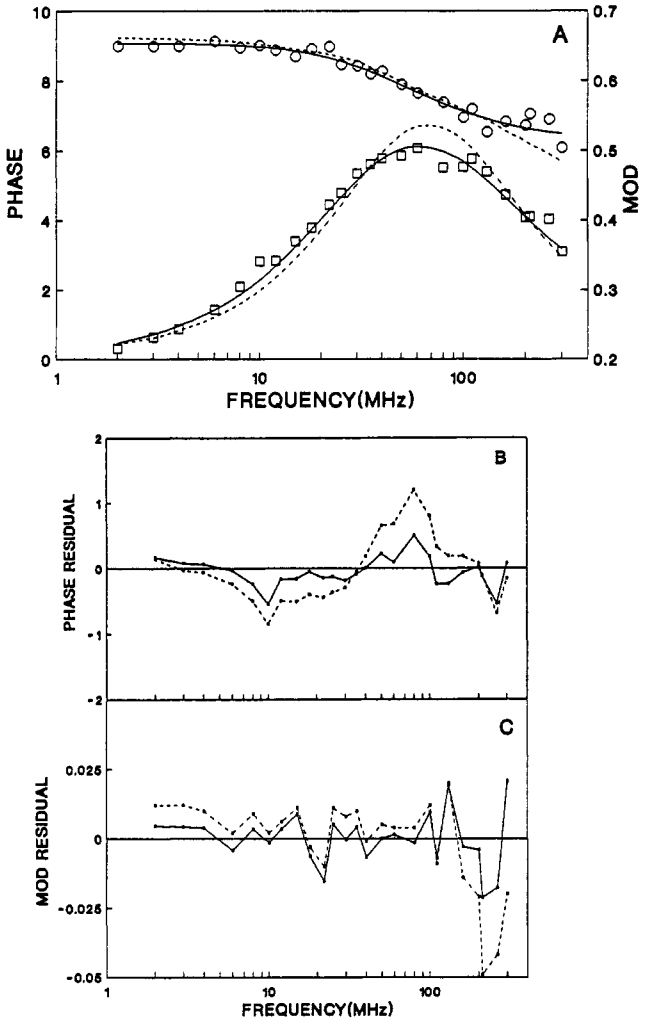

FIGURE 1: Differential polarized phase angle (□) and ratio of polarized modulation (○) as a function of modulation frequency for DPH-PC in DOPE at 30 °C (panel A). The solid and dotted lines were obtained from the P2HOP and P2 fits, respectively. Also the residuals (= differences between experimental and theoretical values) of the differential polarized phase angle (panel B) and the ratio of polarized modulation (panel C) for the P2HOP (solid line) and P2 (dotted line) fits are also shown.

DOPE and DOPC at 30 °C. The fitted phase and modulation values from the P2 and P2HOP fits are also shown in Figure 1A. The fitted values from the P2P4 and P2P4HOP are not shown for clarity. To further examine the goodness of fit, the residues, which are defined as the differences between the theoretical and experimental values, of phase and modulation for both fits are presented as a function of modulation frequency in Figure 1B,C. It is clear that the residues from the P2HOP fit are smaller than those from the P2 fit at most modulation frequencies. As discussed under Materials and Methods, the P2P4HOP is a general model which can describe

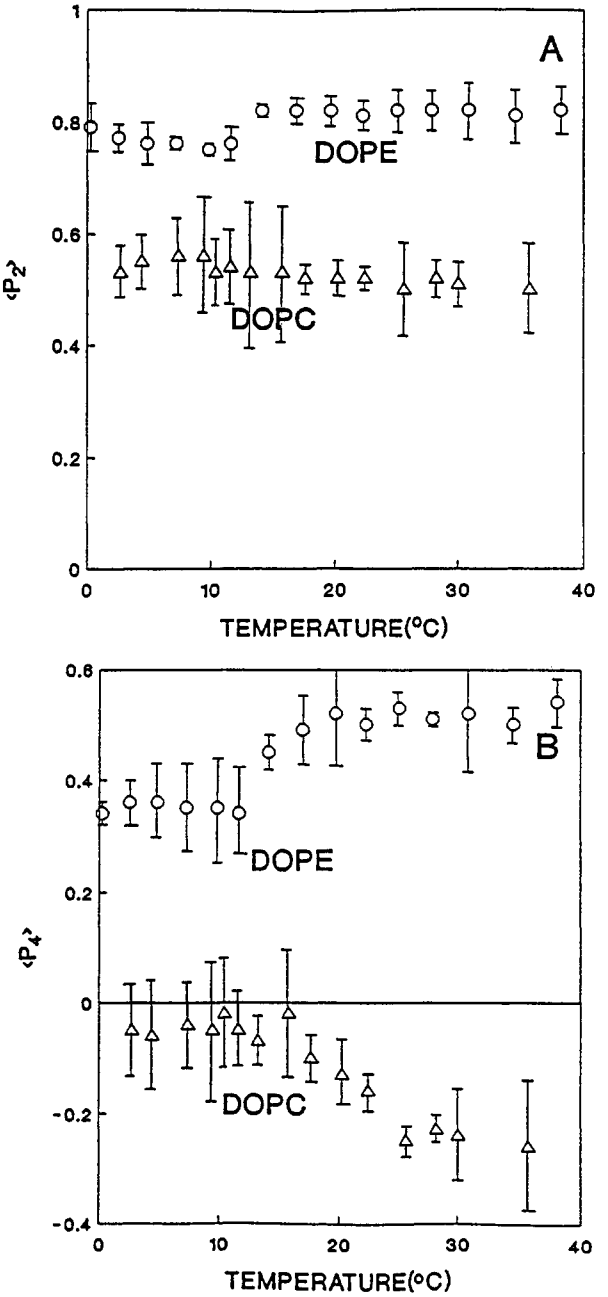

FIGURE 2: Second rank (panel A) and fourth rank (panel B) order parameters vs temperature for DPH-PC in DOPE (○) and DOPC (△). Bars indicate fitting errors.

the anisotropy decay behavior of a fluorophore in both the L_α and H_{II} phases. Therefore only the molecular dynamics parameters obtained from the P2P4HOP model are presented in this study.

The values of the fitted second ($\langle P_2 \rangle$) and fourth ($\langle P_4 \rangle$) rank order parameters of DPH-PC in DOPE and DOPC as

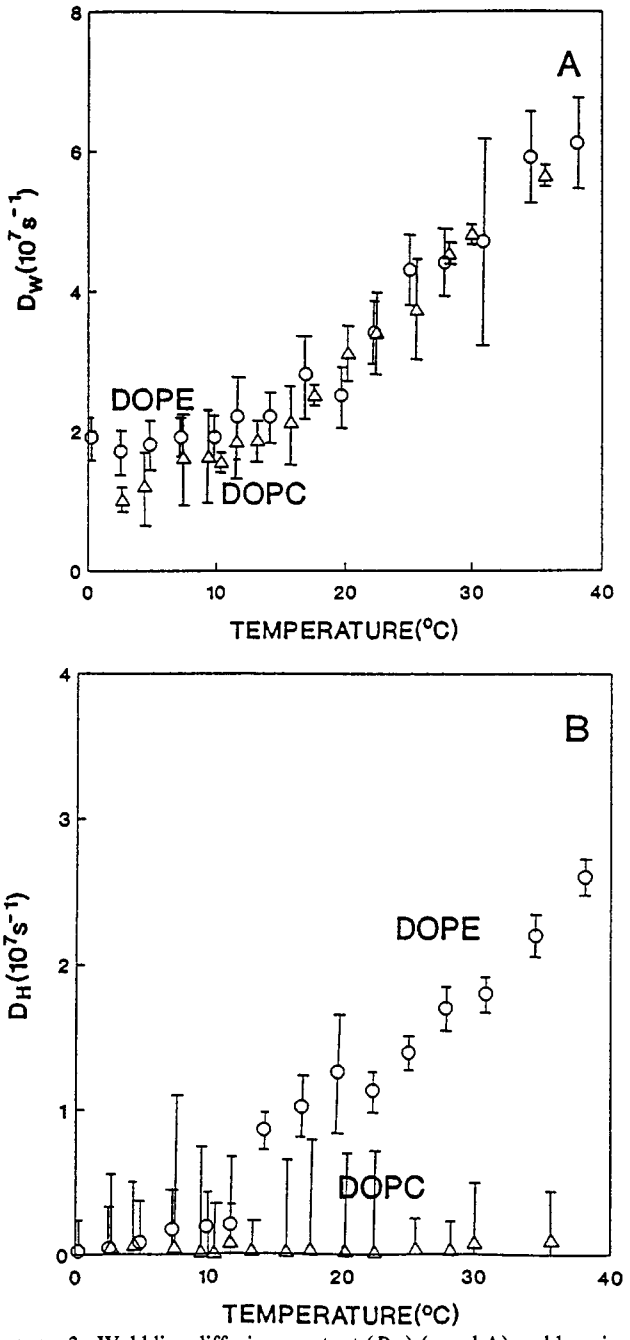

FIGURE 3: Wobbling diffusion constant (D_W) (panel A) and hopping diffusion constant (D_H) vs temperature for DPH-PC in DOPE (○) and DOPC (△). Bars indicate fitting errors.

a function of temperature are shown in Figure 2. In DOPE, an increase in the values of $\langle P_2 \rangle$ and $\langle P_4 \rangle$ at 12–14 °C was evident. In contrast, no significant change in the values of $\langle P_2 \rangle$ was found at all temperatures for DOPC. Yet a broad decrease in the values of $\langle P_4 \rangle$ was observed at 10–30 °C for DOPC. The order parameters of DPH-PC in DOPE were significantly higher than that in DOPC at all temperatures (0–40 °C).

The values of the two fitted rotational diffusion constants, D_W and D_H, of DPH-PC in DOPE and DOPC as a function of temperature are shown in Figure 3. The values of D_W for DOPE were slightly higher than that for DOPC at low temperatures ($T < 10$ °C). At higher temperatures, the values of D_W in both lipids were roughly identical. A prominent increase in the values of D_H from 0 to 0.8×10^7 s^{-1} was observed for DOPE at 12 °C. Thereafter, the values of D_H increased steadily with temperature. In contrast, the values of D_H remained essentially zero for DOPC at all temperatures.

Lateral Diffusion Measurements for DOPE and DOPC. Using fluorescence excimer formation technique, the lateral diffusion constants (D_L) of the lipids in DOPC and DOPE were determined as a function of temperature. The values of the monomer fluorescence lifetimes of PyPC at two different concentrations, 0.05 and 2 mol %, are shown in Figure 4A (DOPC) and Figure 4B (DOPE). Using eq 16, the values of D_L for DOPC and DOPE were calculated from these monomer lifetimes and are shown in Figure 4C. The values of D_L for DOPE were found to be slightly lower than that for DOPC at temperatures lower than 12 °C. Yet these values of D_L for both lipids became indistinguishable higher temperatures.

Interfacial Radius of Curvature (R) Estimations for DOPE and DOPC. On the basis of the relationship between the hopping and lateral diffusion constants (see eq 6), the values of R for DOPE were estimated and are presented in Figure 5. The values of R were found to decrease steadily from 20 Å at 15 °C to 17 Å at 35 °C.

Orientational Dynamics of Binary DOPE/DOPC Lipid Mixtures. Identical frequency-domain fluorescence measurements were also performed on the DOPE/DOPC binary mixtures with DOPE content varying from 0 to 100 mol % and at 3 and 23 °C. The fluorescence lifetimes of DPH-PC (0.1%) in these lipid mixtures were found to be ~6.0 ns and insensitive to both lipid composition (0–100% DOPE) and temperature (3 and 23 °C).

The fitted $\langle P_2 \rangle$ and $\langle P_4 \rangle$ values of DPH-PC in the DOPE/DOPC mixtures as a function of DOPE content are shown in Figure 6. At 23 °C, an increase in the values of $\langle P_2 \rangle$ and $\langle P_4 \rangle$ at 90% DOPE is clearly evident. In contrast, a progressive increase in the values of $\langle P_2 \rangle$ and $\langle P_4 \rangle$ as a function of DOPE content was found at 3 °C.

The values of the two fitted rotational diffusion constants, D_W and D_H, of DPH-PC in the DOPE/DOPC mixtures as a function of DOPE content are shown in Figure 7. At 3 °C, the values of D_W for the DOPE/DOPC mixtures were found to decrease slightly with increasing DOPE content. Yet a decline in the values of D_W was observed as the DOPE content was higher than 85% at 23 °C.

The values of D_H remained essentially zero for all lipid compositions at 3 °C and for DOPE contents less than 85% at 23 °C. However, an abrupt increase in the values of D_H to $\sim 1.2 \times 10^7$ s^{-1} was found as the DOPE content was higher than 85% at 23 °C.

The values of D_L of the lipids in the DOPE/DOPC mixtures at different DOPE contents at 23 °C were also determined by using the pyrene excimer formation technique. The values of D_L were found to decrease slightly (~10%) as the PE content was increased from 0 to 100% and are shown in Figure 8. The radii of curvature of the lipid/water interface (R) of the DOPE/DOPC mixtures (DOPE content greater than 85%) were also determined from the values of D_L and D_H using the relationship of $D_H = (D_L/R^2)$. The values of R for the DOPE/DOPC mixtures at 23 °C with high DOPE contents (>85%) were found to be about 20 Å.

Reconstruction of Orientational Distribution Function. Based on the experimentally recovered order parameters, $\langle P_2 \rangle$ and $\langle P_4 \rangle$, the orientational distribution functions [$f(\theta)$] of DPH-PC in the lipid systems were reconstructed. The reconstructed orientational distribution functions $f(\theta)$ of DPH-PC in the DOPE/DOPC mixtures with varying DOPE content are plotted in Figure 9. At 3 °C, the peak of the orientational distribution was located at about 32° for DOPC. This peak decreased gradually as the DOPE content of the

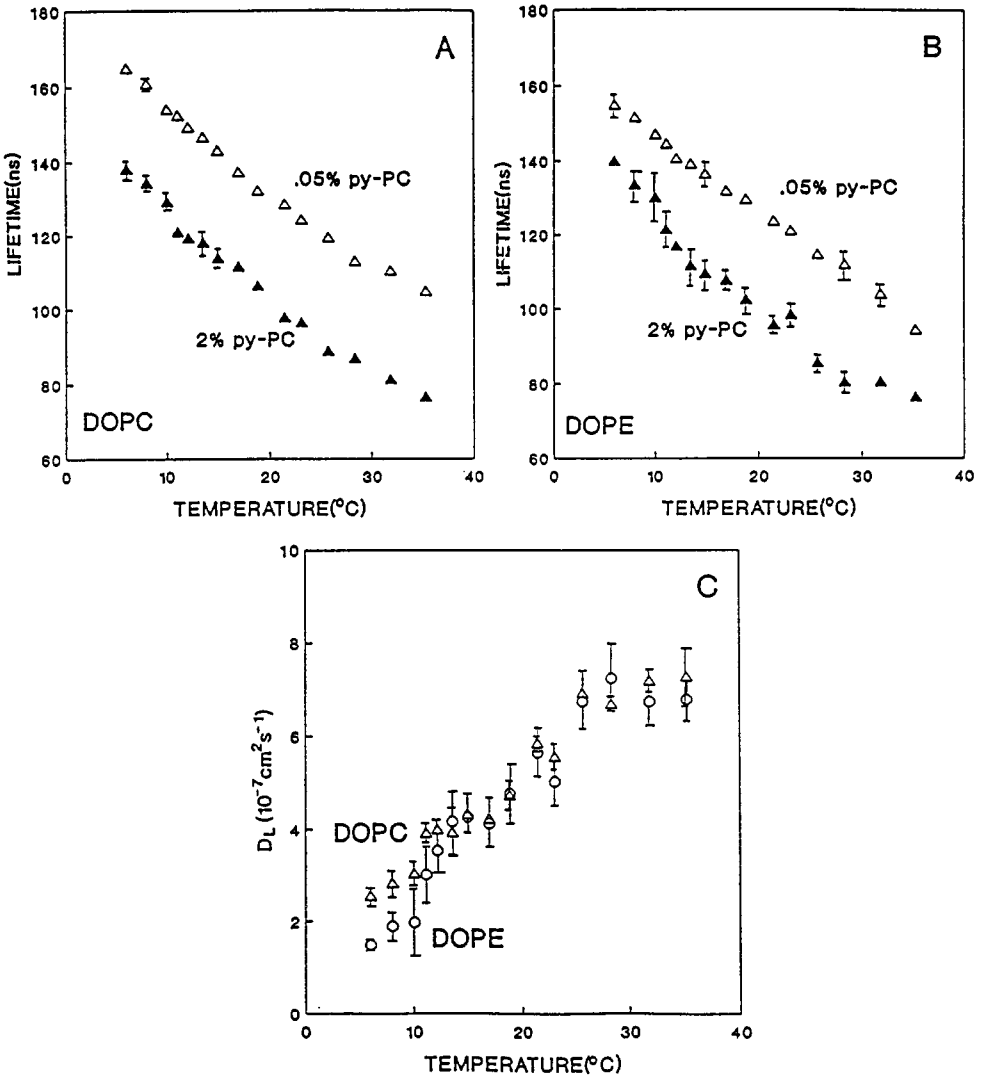

FIGURE 4: Fluorescent lifetime of pyrene monomer emission vs temperature for 0.05% (△) and 2% (▲) PyPC in DOPC (panel A) and in DOPE (panel B). The calculated lateral diffusion constant D_L as a function of temperature for PyPC in DOPE (○) and DOPC (△) is shown in panel C. Bars indicate fitting errors.

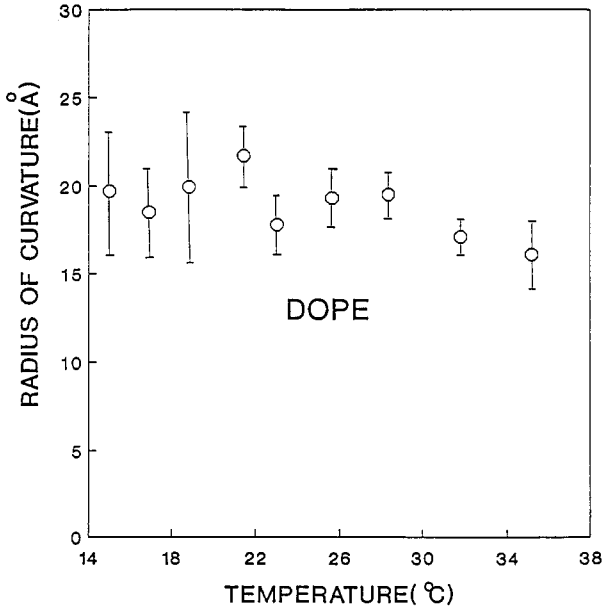

FIGURE 5: Radius of curvature of the lipid/water interface vs temperature for DOPE. Bars indicate fitting errors.

DOPE/DOPC mixtures was increased. At 100% DOPE, the peak was found at 20°. At 23 °C, a similar dependence of the peak location with DOPE content was observed for 0–80% DOPE. However, as the DOPE content reached 100%, the peak shifted dramatically to 0°.

Discussion

Various structural and rotational parameters of DPH-PC in fully hydrated DOPE, DOPC, and their mixtures, which exhibit well-defined L_α and H_{II} phases, have been calculated and compared. Similar to other spectroscopic techniques, e.g., NMR (Fenske et al., 1990; Pastor et al., 1988), theoretical models are required to extract meaningful parameters from the frequency-domain anisotropy data. A newly developed rotational diffusion model (Van Der Meer et al., 1990), P2P4HOP, for describing the fluorescence anisotropy behavior of a cylindrical fluorophore in both the L_α and H_{II} phases was employed in this study.

An extrinsic fluorophore DPH-PC was used in this study. DPH-PC is a fluorescent lipid in which the *sn*-2 chain consists of a DPH moiety. The orientational dynamics of the DPH-PC should be sensitive to the intermolecular constraint imposed by the host lipids on the whole DPH-PC's *sn*-2 chain including the region near the glycerol backbone where the DPH is attached (Cheng, 1989a). DPH has been shown to be a self-quenching fluorophore (Parente & Lentz, 1985). This self-quenching characteristic will manifest itself in the form of reduced fluorescence lifetime if the DPH-PC lipids are aggregated in the lipid layer. No significant alterations in the

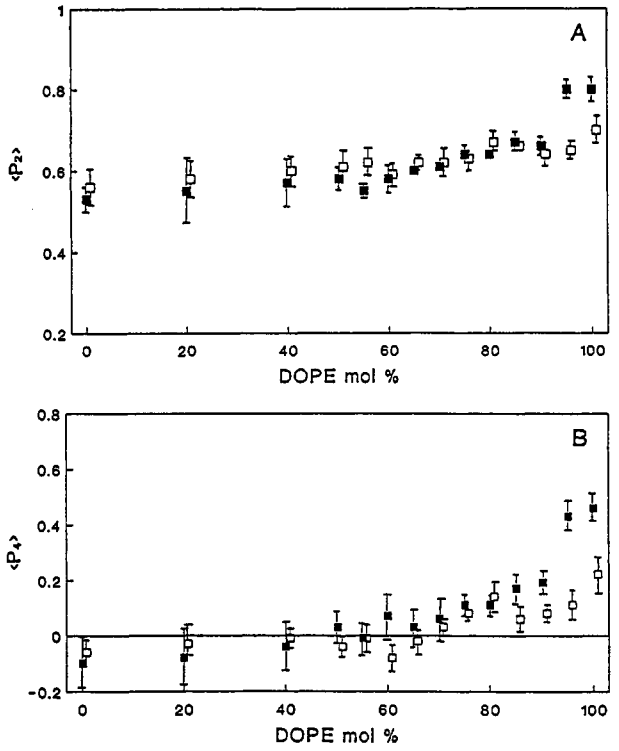

FIGURE 6: Second rank (panel A) and fourth rank (panel B) order parameters vs DOPE content for DPH-PC in DOPE/DOPC mixtures at 3 °C (□) and 23 °C (■). Bars indicate fitting errors.

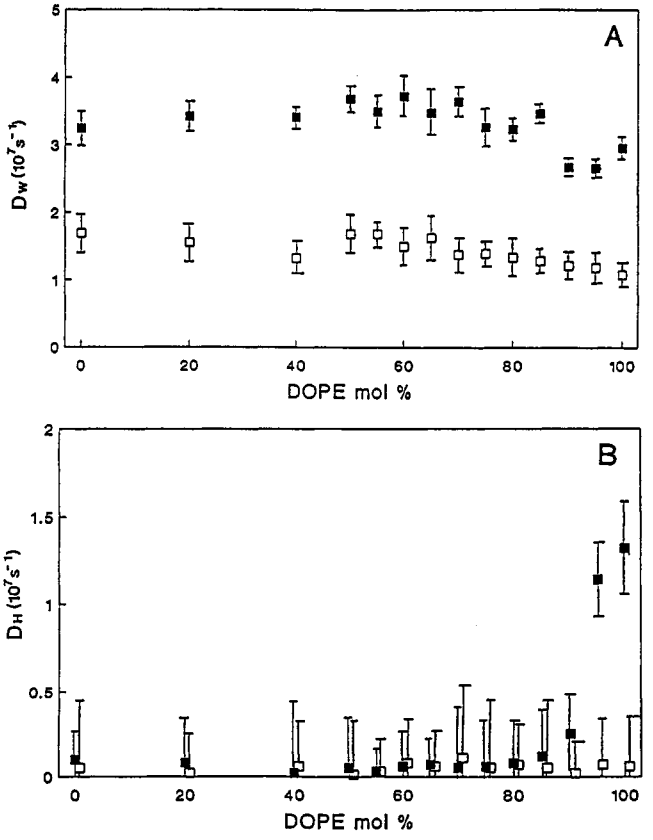

FIGURE 7: Wobbling diffusion constant (D_W) (panel A) and hopping diffusion constant (D_H) (panel B) vs DOPE content for DPH-PC in DOPE/DOPC mixtures at 3 °C (□) and 23 °C (■). Bars indicate fitting errors.

fluorescence lifetimes of DPH-PC were detected in all the lipid systems we studied as a function of either temperature or lipid composition. These results suggested that the DPH-PC molecules are well-mixed with the host lipids.

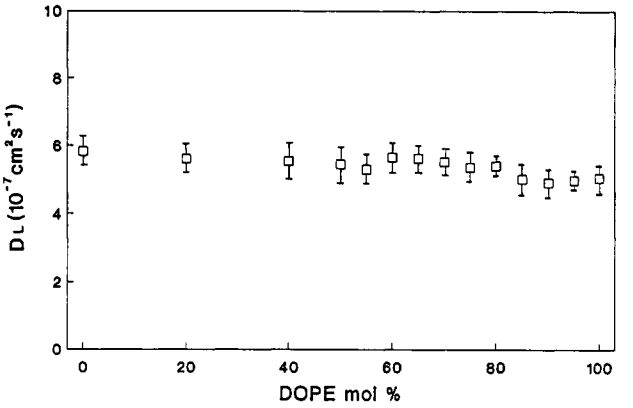

FIGURE 8: Lateral diffusion constant (D_L) of DPH-PC in the DOPE/DOPC mixtures as a function of DOPE content at 23 °C. Bars indicate fitting errors.

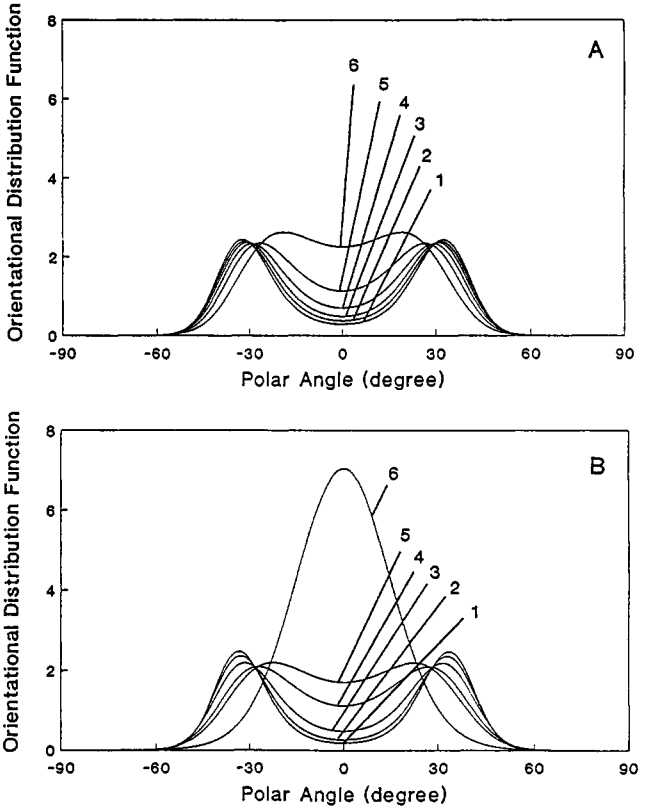

FIGURE 9: Orientational distribution function $f(\beta)$ vs polar angle β for DPH-PC in DOPE/DOPC mixtures with DOPE content of 0% (1), 20% (2), 40% (3), 60% (4), 80% (5), and 100% (6) at 3 °C (panel A) and 23 °C (panel B).

Significant changes in the curvature-related hopping diffusion constants (D_H) of DPH-PC in our model lipid systems have been demonstrated. Here D_H is related to both the translational diffusion constant D_L of the lipids and the radius of curvature R of the lipid layers by the formula $D_H = D_L/R^2$ (see eq 6). Our PyPC data revealed that the values of D_L in DOPE and DOPC are almost identical at all temperatures. Similar observations were also found for DOPE/DOPC mixtures at all DOPE contents. Therefore the changes in D_H are mainly attributed to the alterations in the local curvature of the lipid layer. On the basis of this consideration, the findings of the negligibly small values of D_H for DOPC at 0–40 °C, DOPE at 0–12 °C, and DOPE/DOPC (DOPE >85% at 23 °C and all DOPE contents at 3 °C) are interpreted as the lack of a significant interfacial curvature of those lipids at the mentioned temperatures and compositions. On the other hand, the increase in the values of D_H for DOPE at temperatures

higher than 12 °C and for DOPE/DOPC (DOPE >85% at 23 °C) signifies a temperature- and composition-induced increase in the interfacial curvature of the lipids, respectively. Interestingly, all these thermotropic and lyotropic L_α–H_{II} phase transitions have been confirmed previously on the basis of the noninvasive X-ray diffraction (Gruner, 1989, and references therein) and Fourier transform infrared (FTIR) measurements (Cheng, 1991). We therefore concluded that the hopping diffusion parameter D_H is very sensitive to the formation of nonlamellar phases of nonzero curvatures.

The validity of the P2P4HOP model can be tested by comparing our calculated curvature parameters of the lipids with the X-ray diffraction results. On the basis of our fluorescence data, the calculated values of R in the H_{II} phase fall into the range of 17–20 Å. As described under Materials and Methods, R is defined from the center of the hexagonally packed lipid tube to the center of emission dipole moment of DPH. On the basis of the space filling model of DPH-PC (Parente & Lentz, 1985), the radius of the water core (R_W) inside the lipid tube is roughly 5–10 Å less than the value of R. Note that the lipid/water interface is assumed to be located at the glycerol backbone not at the top of the lipid head group (Rand et al., 1990). On the basis of the above argument, our estimated range of R_W is 7–15 Å and in the same order of magnitude as the result obtained from a recent X-ray diffraction experiment on fully hydrated DOPE (Tate & Gruner, 1989). The latter predicted a larger range of R_W (20–22 Å). Considering the assumptions stated in the theoretical model as described under Materials and Methods, we believe that the match of the order of magnitude of R_W from our indirect fluorescence method with that from the direct X-ray method is quite satisfactory. We therefore concluded that the P2P4HOP model (Van Der Meer et al., 1990) is appropriate and adequate in describing the orientational dynamics of the lipids in both the L_α and H_{II} phases.

The orientational distribution function $f(\theta)$ of DPH-PC has been reconstructed from the recovered values of $\langle P_2 \rangle$ and $\langle P_4 \rangle$. It is interesting to mention that extra sets of $\langle P_2 \rangle$ and $\langle P_4 \rangle$ were obtained from the fitting procedure other than those presented in Figure 2A,B. These occurred for DOPC at some temperatures and for DOPE exclusively at low temperatures (<11 °C). This nonuniqueness of $\langle P_2 \rangle$ and $\langle P_4 \rangle$ has also been reported for various lipid systems by using DPH as the probe (Ameloot et al., 1984; Wang et al., 1991). For DOPC, the reconstructed orientational distribution functions based on these extra sets of $\langle P_2 \rangle$ and $\langle P_4 \rangle$ exhibited bimodal behavior with peaks at 0° and at 90°. The peak at 90° corresponds to the presence of a certain population of the probe molecules at the center of the two lipid monolayers and with their long axes parallel to the surface of the bilayer. The above bimodal distribution is generally expected for the hydrophobic DPH probes. Yet this bimodal distribution is not possible for our amphiphilic DPH-PC probes (Cheng, 1989a,b). Besides the above argument of the amphiphilic versus hydrophobic nature of the probes, the values of χ_R^2 associated with these extra sets of $\langle P_2 \rangle$ and $\langle P_4 \rangle$ are generally 2–3-fold larger than those associated with the sets reported in the figures. In addition, for DOPE, the new sets of $\langle P_2 \rangle$ and $\langle P_4 \rangle$ were always associated with negative values of D_H, which are physically meaningless. Therefore the extra sets of $\langle P_2 \rangle$ and $\langle P_4 \rangle$ of DPH-PC in this study were rejected.

The question of how the molecular dynamics parameters obtained from this fluorescence study provide insights into understanding the existence of lateral stress in the lipid layer containing nonbilayer phase preferring lipids needs to be answered. According to a recently proposed *stress* model (Gruner, 1989; Seddon, 1990), a lipid monolayer consisting of nonbilayer phase (H_{II}) preferring lipids has a characteristic nonzero spontaneous curvature. Confining this monolayer into a planar form results in a high elastic free energy stored in the lipids and gives rise to a lateral stress in the lipid layer. This is analogous to bending an intrinsically curved rubber into a planar sheet. The energy used for bending is stored in a form of elastic potential energy within the rubber. Owing to the presence of other competing free energy terms, such as electrostatic, hydration, and hydrocarbon packing, the monolayer may retain in the planar bilayer (L_α) phase at the expense of a high elastic energy. Thus the lipid layer containing nonbilayer phase preferring lipids may experience a larger lateral pressure or stress in the bilayer than that containing bilayer phase preferring lipids. In our case, DOPE is the nonbilayer phase preferring lipid, while DOPC is the bilayer phase preferring lipid.

It is our working hypothesis that an increase in the lateral stress should result in a tighter packing of the lipids across the lipid layer. The lateral stress in the bilayer containing nonbilayer phase preferring lipids may be quantitated by monitoring the change in the orientational distribution functions of DPH-PC in DOPE/DOPC mixtures in the L_α phase (0–100% DOPE at 3 °C and 0–80% DOPE at 23 °C). It is evident that the peak of the orientational distribution function shifts significantly toward the normal of the lipid/water interface as the content of DOPE increases. This observation indicated that the lateral stress starts to build up in response to the increasing amount of nonbilayer phase preferring lipids in the bilayer. It is interesting to mention that a recent FTIR study (Cheng, 1991) on the CH_2 and C=O vibrations of the same DOPE/DOPC mixtures also indicated that the lipids are more tightly packed in the hydrocarbon and lipid/water interfacial regions as the content of DOPE increases.

Our results also indicated that DPH-PC is slightly more oriented toward the lipid/water interface normal in the H_{II} phase than in the L_α phase. Furthermore, the distribution function exhibits a peak at nonzero polar angle in the L_α phase but at zero polar angle in the H_{II} phase. Apparently, in the L_α phase, the lipid acyl chains wobble around an orientation that is tilted away from the normal of the lipid/water interface, whereas in the H_{II} phase these chains wobble around the interface normal itself. In addition, the wobbling diffusion motion of DPH-PC is significantly lower in the H_{II} phase than that in the L_α phase. These results led us to conclude that a higher intermolecular constraint is imposed on the lipids in the curved lipid layers than in the planar layers. However, it is known that the amount of gauche rotamers of the lipid acyl chains increases rather than decreases at the L_α–H_{II} transition (Cheng, 1991, and references therein). Therefore the higher local orientational order and the more restricted wobbling motion of DPH-PC in the H_{II} phase must be attributed to the higher packing constraint imposed on the lipids near the glycerol backbone region. Note that the above proposed tighter packing at the glycerol backbone region of the lipids in the H_{II} phase has been confirmed by the observed increase in the infrared C=O stretching frequency of the lipids at the lyotropic L_α–H_{II} phase transition of the same DOPE/DOPC mixtures (Cheng, 1991).

It is important to mention that our radius of curvature parameter decreases with increasing temperature for DOPE. This may be related with a decrease in R_W with temperature, assuming that the thickness of the lipid layers in the H_{II} phase is insensitive to temperature. The above prediction is in accord

with the theoretical prediction that the elastic and hydrocarbon packing energy terms both decrease with decreasing R_W (Gruner, 1989).

In summary, our P2P4HOP model is valid in describing the local dynamics and orientation of the lipids in the L_α and H_{II} phases. The calculated parameter D_H allows us for the first time to detect and quantitate the change in the local curvature of the lipid layers using frequency-domain fluorescence anisotropy technique. The local orientational distribution function of DPH-PC allows us to demonstrate the existence of lateral stress in the lipid layer containing nonbilayer phase preferring lipids.

Registry No. DOPE, 4004-05-1; DOPC, 4235-95-4; DPH-PC, 98014-38-1.

References

Ameloot, M., Hendrick, H., Herreman, W., Pottel, H., Cauwelaert, F. V., & Van Der Meer, W. (1984) *Biophys. J. 46*, 525–539.

Berne, B. J., Pechukas, P., & Harp, G. D. (1968) *J. Chem. Phys. 49*, 3125–3132.

Chen, S.-Y., Cheng, K. H., Van Der Meer, B. W., & Beechem, J. M. (1990a) *Biophys. J. 58*, 1527–1537.

Chen, S.-Y., Cheng, K. H., & Ortalano, D. M. (1990b) *Chem. Phys. Lipids 53*, 321–330.

Cheng, K. H. (1989a) *Biophys. J. 55*, 1025–1031.

Cheng, K. H. (1989b) *Chem. Phys. Lipids 51*, 137–145.

Cheng, K. H. (1989c) Fluorescence Detection III (Menzel, E. R., Ed.) *Proc. SPIE Int. Soc. Opt. Eng. 1054*, 160–167.

Cheng, K. H. (1991) *Chem. Phys. Lipids 60*, 119–125.

Cheng, K. H., & Hui, S. W. (1986) *Arch. Biochem. Biophys. 244*, 382–386.

Chong, P. L., & Thompson, T. E. (1985) *Biophys. J. 47*, 613–621.

Deinum, G., van Langen, H., van Ginkel, G., & Levine, Y. K. (1988) *Biochemistry 27*, 852–860.

Fenske, D. B., Jarrell, H. C., Guo, Y., & Hui, S. W. (1990) *Biochemistry 29*, 1222–1229.

Galla, H.-J., Hartmann, W., Theilen, U., & Sackmann, E. (1979) *J. Membr. Biol. 48*, 215–236.

Gratton, E., Jameson, D. M., & Hall, R. D. (1984) *Annu. Rev. Biophys. Bioeng. 13*, 105–124.

Gruner, S. M. (1989) *Phys. Chem. 93*, 7562–7570.

Jaynes, E. T. (1983) *Papers on Probability, Statistics and Statistical Physics* (Rosenkrantz, R. D., Ed.) D. Reidel Publishing Co., Boston.

Lakowicz, J. R. (1983) *Principle of Fluorescence Spectroscopy*, pp 126–128, Plenum Press, NY.

Luzzati, V., & Husson, F. (1962) *J. Cell Biol. 12*, 207–219.

Parente, R. A., & Lentz, B. R. (1985) *Biochemistry 24*, 6178–6185.

Pastor, R. W., Venable, R. M., Karplus, M., & Szabo, A. (1988) *J. Chem. Phys. 89*, 1128–1140.

Rand, R. P., Fuller, N. L., Gruner, S. M., & Parsegian, V. A. (1990) *Biochemistry 29*, 76–87.

Seddon, J. M. (1990) *Biochim. Biophys. Acta 1031*, 1–69.

Spencer, R. D., & Weber, G. (1970) *J. Chem. Phys. 52*, 1654–1663.

Szabo, A. (1984) *J. Chem. Phys. 81*, 150–168.

Tate, M. W., & Gruner, S. M. (1989) *Biochemistry 28*, 4245–4253.

Van Der Meer, W. B., Pottel, H., Herreman, W., Ameloot, M., Hendrick, H., & Schröder, H. (1984) *Biophys. J. 46*, 515–523.

Van Der Meer, B. W., Cheng, K. H., & Chen, S.-Y. (1990) *Biophys. J. 58*, 1518–1526.

Van Langen, H., Schrama, D. A., van Ginkel, G., Ranke, G., & Levin, Y. K. (1989) *Biophys. J. 55*, 937–947.

Wang, S., Beechem, J. M., Gratton, E., & Glaser, M. (1991) *Biochemistry 30*, 5565–5572.

Weber, G. (1977) *J. Chem. Phys. 66*, 4081–4090.

Zannoni, D., Arcioni, A., & Cavatorta, P. (1983) *Chem. Phys. Lipids 32*, 179–196.